Macromolecules

ARTICLE

pubs.acs.org/Macromolecules

Interaction of Microstructure and Interfacial Adhesion on Impact Performance of Polylactide (PLA) Ternary Blends

Hongzhi Liu,[†] Wenjia Song,[†] Feng Chen,[†] Li Guo,[‡] and Jinwen Zhang*[,†]

[†]Composite Materials and Engineering Center, Washington State University, Pullman, Washington 99164, United States

[‡]Department of Chemistry and Macromolecular Studies Group, Louisiana State University, Baton Rouge, Louisiana 70803, United States

Supporting Information

ABSTRACT: Polyactide (PLA) was blended with an ethylene/*n*-butyl acrylate/glycidyl methacrylate (EBA-GMA) terpolymer and a zinc ionomer of ethylene/methacrylic acid (EMAA-Zn) copolymer. The phase morphology of the resulting ternary blends and its relationship with impact behaviors were studied systematically. Dynamic vulcanization of EBA-GMA in the presence of EMAA-Zn was investigated by torque rheology, and its cross-link level was evaluated by dynamic mechanical analysis. Reactive compatibilization between PLA and EBA-GMA was studied using Fourier transform infrared spectroscopy. The dispersed domains in the ternary blends displayed a "salami"-like phase structure, in which the EMAA-Zn phase evolved from occluded subinclusions into continuous phase with decrease in the EBA-GMA/EMAA-Zn ratio. An optimum range of particle sizes of the dispersed domains for high impact toughness was identified. Also, the micromechanical deformation process of these ternary blends was also investigated by observation of the impact-fractured surfaces using the electron microscope. It was suggested that the low cavitation resistance of dispersed particles in conjunction with suitable interfacial adhesion was responsible for the optimum impact toughness observed.

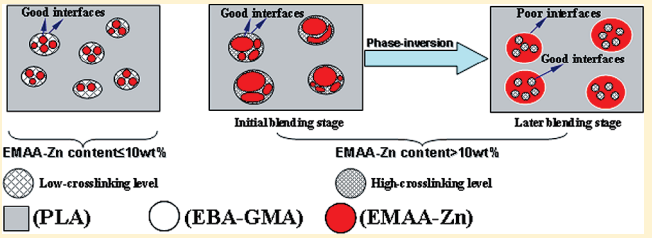

1. INTRODUCTION

Among various commercial biodegradable polymers, polylactide (PLA) continues to gain its market share due to its renewability, competitive cost, high strength, modulus and transparency, etc. Nonetheless, one of its major drawbacks, brittleness, still remains the main research focus in both industry and academia. Among various modifications, melt blending is the most economic means to improve its toughness. Until now, various biodegradable or nonbiodegradable polymers, such as poly(butylene adipate-*co*-terephthalate),[1,2] polycaprolactone,[3,4] polyhydroxyalkanoate copolymers,[5,6] poly(butylene succinate),[7,8] hyperbranched polymers,[9−11] poly(ether)urethane elastomer,[12] polyamide elastomer,[13] soybean oil derivatives,[14,15] thermoplastic polyolefin elastomer,[16] rubbers,[17] acrylonitrile−butadiene−styrene copolymer,[18] polyethylene,[19,20] poly(ethylene−glycidyl methacrylate),[21] and glycidyl methacrylate-grafted poly(ethylene−octene),[22] have been used as toughening modifiers for PLA. Although the majority of the above modifiers alone[1,8,12,13,22] or in combination with a compatibilizer[2−4,7] tended to result in a remarkable increase in tensile toughness (ductility) of PLA, they only demonstrated limited improvement on impact toughness in the notched state. When the reactive modifiers were used,[21,22] only the compatibilizing reactions at the interface between the dispersed and the matrix phases were involved. Even though a few supertoughened PLA blends (>530 J/m of notched impact strength[23]) were reported,[19−21] a comprehensive understanding of the relationship between toughness and morphology is lacking at present.

It is well-known that the size and substructure of the dispersed rubber modifier play a crucial role in determining the ultimate toughening effect and the deformation mechanism.[24] The existence of an optimum particle size has been reported in various rubber-toughened thermoplastic polymer systems.[23,25−34] There is general agreement that the lower size limit is attributed to the fact[29,33,35−38] that very small rubber particles are inefficient for cavitation, whereas the upper rubber size limit that has been associated with a critical interparticle distance still remains a controversial topic.[35] Dompas and Groeninckx[29] developed criteria for internal cavitation of rubber particles and suggested that the critical rubber particle size was 100−200 nm. This concept of critical particle size was used to explain the decrease in toughening efficiency for different rubber-modified blend systems involving very small particles. On the basis of stress-whitening analysis and TEM observation during uniaxial tensile testing, they concluded that the resistance to cavitation increased with decreasing rubber particle size.[36] They further combined the concepts of critical particle size and critical interparticle distance to explain the observed optimum size in rubber-toughened poly(methyl methacrylate) (PMMA) and poly(vinyl chloride)

Received: November 25, 2010
Revised: January 28, 2011
Published: February 16, 2011

Scheme 1. Illustration of the Chemical Structure of the Three Polymers

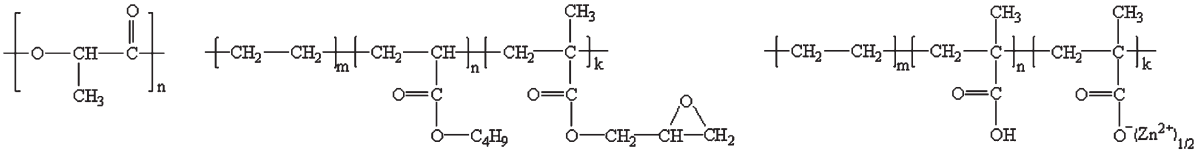

Table 1. Characteristics of Materials

polymer (abbreviation)	grade (supplier)	specifications
polylactide (PLA)	PLA2002D (NatureWorks LLC)	MI (210 °C, 2.16 kg) = 5−7 g/10 min; specific gravity = 1.24
ethylene/*n*-butyl acrylate/glycidyl methacrylate terpolymer (EBA-GMA)	Elvaloy PTW (DuPont Co.)	MI (190 °C, 2.16 kg) = 12 g/10 min; specific gravity = 0.94; melting point (DSC) = 72 °C; E/BA/GMA = 66.75/28/5.25 (wt %)[41]
zinc ionomer of ethylene/methacrylic acid copolymer (EMAA-Zn)	Surlyn 9945 (DuPont Co.)	MI (190 °C, 2.16 kg) = 4.0 g/10 min; specific gravity = 0.97; melting point (DSC) = 89 °C; methacrylic acid content = 15.0 wt %; zinc oxide content = 3.70 wt %; neutralization = ∼40%[42]

(PVC) systems.[29,33] Very recently, Bucknall and Paul[35] introduced a new model to explain the observed relationship between particle size and fracture resistance in nylon/rubber blends. Model calculations showed that the critical volume strain at cavitation increased as the particle size was reduced. They argued that maximum toughness was achieved when the particle size was large enough to cavitate ahead of a notch or crack tip, but not so large as to initiate unstable crazes and thereby reduce fracture resistance. It is worth mentioning that very small particles are not always inefficient for cavitation in some toughened thermosetting blend systems since nanocavitation of well-dispersed nanoscale spherical micelles (∼15 nm) in self-assembled amphiphilic block copolymer-modified epoxy has been noted by Liu et al.[39]

We recently reported a novel PLA ternary blend system consisting of an ethylene/*n*-butyl acrylate/glycidyl methacrylate terpolymer elastomer (EBA-GMA) and a zinc ionomer of ethylene/methacrylic acid copolymer (EMAA-Zn).[40] TEM observations revealed that the "salami"-like substructure was formed in the ternary blends. When the elastomer/ionomer ratio was equal to or larger than 1 and the extrusion blending was performed at 240 °C, supertoughened blends were achieved. This reactive blending involved simultaneous vulcanization (cross-linking) of EBA-GMA and interfacial reactive compatibilization between PLA and EBA-GMA. Effective interfacial compatibilization at elevated blending temperatures was thought to be responsible for the significant increase in notched impact strength. In addition, dynamic vulcanization induced by the addition of EMAA-Zn led to the cross-linking of the rubbery EBA-GMA phase and was thereby expected to alter the stiffness and the particle size of the dispersed phase.

However, what is still unknown are how compatibilization and dynamic vulcanization is governed by the elastomer/ionomer ratio and how the resulting changes in the microstructure of the dispersed particles and interfacial adhesion influences impact behavior of the final blends. To date, there have been no studies in the literature that address the effect of particle size of the dispersed phase on impact behavior of PLA blends and the associated toughening mechanism in relation to the micromechanical deformation process. With these aims in mind, the effects of the elastomer/ionomer ratio on vulcanization and compatibilization in the PLA/EBA-GMA/EMAA-Zn ternary blends and consequently the microstructure of the dispersed particles and their interfacial adhesion with the PLA matrix were investigated in this study. Furthermore, we investigated the effects of particle size of the dispersed domains on impact behavior and explored the dependence of the toughening mechanism on the elastomer/ionomer ratios in the PLA blends. To the best of our knowledge, there have been no similar studies on optimum particle size and the micromechanical deformation process for high impact performance of PLA blends in the literature.

2. EXPERIMENTAL SECTION

2.1. Materials and Sample Preparations. The chemical structures of the three polymers used for the blends are illustrated in Scheme 1, and some relevant information and abbreviations are listed in Table 1. Prior to extrusion, PLA pellets were dried at 80 °C for 1 day in a convection oven and the EMAA-Zn pellets were oven-dried at 75 °C overnight. Melt blending was performed using a corotating twin-screw extruder (Leistritz ZSE-18) with a screw diameter of 17.8 mm and an *L*/*D* ratio of 40 at a screw speed of 50 rpm. The temperature profile of the extruder barrels was 210/220/230/240/240/240/230/220 °C from the first heating zone (next to feeding throat) to die, respectively. For all blends, the weight ratio of EMAA-Zn/EBAGMA was varied in a broad range while the total content of PLA was fixed at 80 wt % on the basis of total blend weight. After being oven-dried, the extruded pellets were injection-molded (Sumitomo SE50D) into ASTM standard specimens at a melt temperature of 190 °C and at a mold temperature of 35 °C. All test specimens were conditioned for 7 days at 23 °C and 50% RH prior to mechanical testing and characterization. For the latter FT-IR analysis, the binary EBA-GMA/EMAA-Zn blends with different weight ratios were also prepared using the same extruder under the same conditions as above.

2.2. Mechanical Test. Tensile tests were conducted on a universal testing machine (Instron 4466) following ASTM D638 (type I specimens). The crosshead speed was 5.08 mm/min, and the initial strain was measured using a 50.8 mm extensometer. Notched Izod impact tests were performed according to ASTM D256 using a BPI-0-1

Basic Pendulum Impact tester (Dynisco, MA). Average test values from five replicated specimens were taken for each sample.

2.3. Torque Rheology. In order to evaluate the effect of blend composition on dynamic vulcanization (cross-linking) between EBA-GMA and EMAA-Zn during compounding, a torque rheometer (Haake Rheomix 600p) was utilized to monitor the mixing torque under the same mixing speed and temperature (i.e., 50 rpm and 240 °C) as the extrusion blending. The polymer mixture was quickly charged into the mixing chamber immediately when the rotors began to rotate. Upon the completion of feeding, the ram was closed and the mixture was allowed to mix for 6 min. This time frame was sufficient to match the residence time in the extrusion blending process. The torque value was recorded as a function of mixing time.

2.4. Dynamic Mechanical Analysis (DMA). Dynamic mechanical properties of the blends were measured with the DMA Q800 (TA Instruments) in a single-cantilever mode with an oscillating frequency of 1 Hz. The temperature was swept from −100 to 150 °C at 3 °C/min. For each sample, duplicated tests were performed in order to ensure the reproducibility of data.

2.5. Morphological Characterization. *2.5.1. Scanning Electron Microscopy (SEM).* In order to analyze the deformation mechanism of the blends, the fractured surfaces of specimens after the Izod impact test were sputter-coated with a thin layer of gold and then examined for morphological structure through a Quanta 200F field emission scanning electron microscope (FE-SEM, FEI Co.) at an accelerated voltage of 15 kV.

2.5.2. Transmission Electron Microscopy (TEM). The morphologies of the dispersed phases were recorded using a transmission electron microscope (TEM, JEOL 1200EX) at an accelerated voltage of 100 kV. Ultrathin sections of ca. 70−80 nm in thickness from the plane perpendicular to the injection flow direction were sliced using a RMC cryo-ultramicrotome equipped with a diamond knife and mounted on Formvar-coated 200-mesh nickel grids. For the purpose of particle size analysis, at least 300 particles from 4−5 independent TEM images were analyzed by a semiautomated image analysis technique based on NIH image software. The cross-sectional area (A_i) of each individual particle (i) was measured and converted into an equivalent diameter of a sphere by the equation ($d_i = (4A_i/\pi)^{0.5}$). Weight-average particle diameter (d_w), which is usually thought to give a better correlation with notched impact toughness than number-average particle diameter (d_n),[43,44] was determined from the following equation

$$d_w = \frac{\sum n_i d_i^2}{\sum n_i d_i} \quad (1)$$

where n_i is the number of particles having the apparent particle diameter d_i. Additionally, particles whose sizes were too small to be measured at the magnification chosen were neglected. Since weight-average particle diameter emphasizes the contribution of large particles, this treatment of the images would not significantly influence final d_w results. Both the ratio of weight-average particle diameter to number-average particle diameter (i.e., d_w/d_n) and the ratio of volume average particle diameter to number-average particle diameter (i.e., d_v/d_n) were used to characterize the polydispersity of particle size. The volume average particle diameter (d_v) was calculated from the following equation:

$$d_v = \frac{\sum n_i d_i^4}{\sum n_i d_i^3} \quad (2)$$

In order to evaluate the micromechanical deformation behavior of selected samples, the impact-fractured specimens were also cryogenically microtomed from the stress-whitening zone immediately underneath the center section of fresh Izod impact fracture surfaces using a diamond knife. A JEOL 1200EX TEM operated at 100 kV was employed.

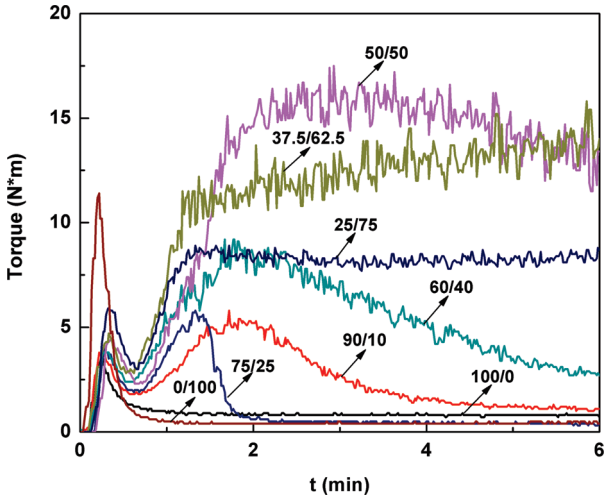

Figure 1. Effect of EMAA-Zn content on melt torque during reactive blending of EBA-GMA/EMAA-Zn binary blends at 240 °C and 50 rpm. The EBA-GMA/EMAA-Zn weight ratios are indicated on the curves.

2.6. Differential Scanning Calorimetry (DSC). Thermal analysis was performed using a Mettler Toledo DSC 822e under an atmosphere of nitrogen. Since it is the original crystalline state of the PLA in the molded samples that determines mechanical properties, only the DSC data from the first heating scan was presented. Specifically, about 5 mg of the sample taken from the cross section at the center of injection-molded specimens was heated to 200 °C at a heating rate of 10 °C/min under nitrogen. The degree of crystallinity (X_c) of the PLA component was determined using the relationship

$$X_c = \frac{\Delta H_m - \Delta H_c}{w_f \Delta H_m^\circ} \times 100\% \quad (3)$$

where ΔH_m and ΔH_c are the enthalpies of melting and cold crystallization during the first heating cycle, respectively; ΔH_m° is the melting enthalpy assuming 100% crystalline PLA (93.7 J/g),[45] and w_f is the weight fraction of PLA in the blend.

2.7. Fourier Transform Infrared Spectroscopy (FT-IR). The absorption spectra were recorded using a Thermo Nicolet Nexus 670 spectrometer with a resolution of 4 cm^{-1} and 32 scans. For the EBA-GMA/EMAA-Zn binary blends, a very small amount of samples was grinded with dried KBr powder and then compressed into disks for the FT-IR test. For each PLA/EBA-GMA/EMAA-Zn blend, the injection-molded blend specimen was first microtomed into slices with ∼120 μm in thickness, followed by the extraction with 1,4-dioxane at ambient temperature under stirring for 10 days to selectively remove free PLA thoroughly. Neat PLA as a control was extracted following the same procedure, and the result showed that neat PLA was completely removed. A small amount of the vacuum-dried insoluble residue was grinded with dried KBr powder and then compressed into disks for the FT-IR test. The FT-IR spectrum of the extracted PLA/EMAA-Zn (80/20, w/w) blend was almost identical to that of pure EMAA-Zn, indicating that PLA did not react with EMAA-Zn and was completely removed under the above extraction conditions. Therefore, the trace of PLA in the extracted ternary blends was believed to result from the grafting of PLA onto EBA-GMA.

All FT-IR samples were oven-dried under a vacuum to eliminate the effects of residual solvent and moisture prior to testing. After the baseline correction, the deconvolution of the bands at ∼1759, ∼1733, and ∼1700 cm^{-1} was well made using the Lorentzian function.

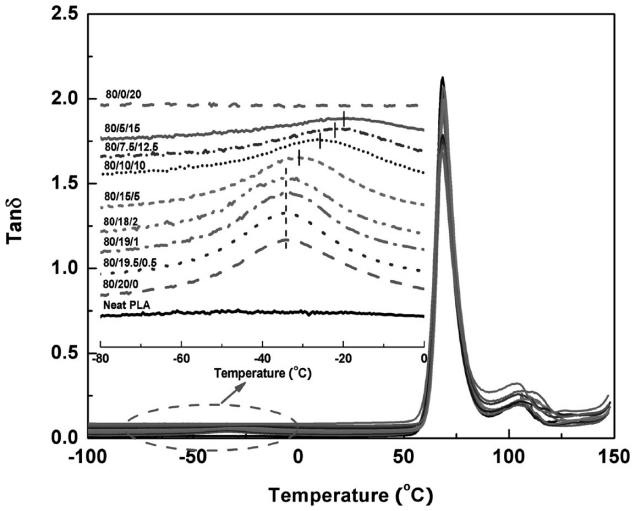

Figure 2. Dependence of damping factor (tan δ) on temperature for various PLA/EBA-GMA/EMAA-Zn (80/20-x/x, w/w/w) ternary blends. Some curves were shifted vertically for clarity.

3. RESULTS AND DISCUSSION

3.1. Dynamic Vulcanization vs Reactive Interfacial Compatibilization. The vulcanization (cross-linking) of the EBA-GMA elastomer was studied using a torque rheometer. Figure 1 shows the torque evolution as a function of mixing time for a series of EBA-GMA/EMAA-Zn binary blends. The initial peak in the torque curve was due to the melting of the polymer pellets. For all binary blends, the torque rise after polymer melting confirmed the occurrence of vulcanization. Additionally, the slope of torque curve increased with the EMAA-Zn loading, indicating faster vulcanization. All binary blends achieved the equilibrium torque values within 3 min. Such time scale was comparable to the residence time under the twin-screw extrusion (50 rpm, 240 °C), suggesting the completion of cross-linking reactions during extrusion blending. When the EMAA-Zn loading was less than 50 wt % in the binary blends, the torque curves showed an initial increase, followed by a gradual decrease. At 50 wt % or higher EMAA-Zn, however, the torque curves became relatively flat after attaining the maximum value. The binary blends with different EBA-GMA/EMAA-Zn weight ratios displayed remarkable differences in appearance. When EBA-GMA was the major component, the final blend crumbled and appeared like spongy agglomerates. When EMAA-Zn was the major component, the final blend still behaved like a thermoplastic. When EBA-GMA was the major component, it acted as the matrix phase during mixing. Given sufficient mixing time, the cross-linking reaction of the EBA-GMA matrix gradually increased to a degree at which the blend lost the melt flowability, and the cross-link network finally crumbled into spongelike agglomerates under shearing action. Correspondingly, torque value decreased with time after reaching the maximum. When the EMAA-Zn content was above 50 wt %, EMAA-Zn became the matrix phase. Consequently, the resulting blends retained melt behaviors of the EMAA-Zn matrix although the EBA-GMA phases could be highly cross-linked due to the presence of more carboxylic acid and zinc groups which served as initiators and catalysts. Again, these results confirmed that cross-linking indeed occurred within the EBA-GMA phase. The maximum equilibrium torque value at 50 wt % EMAA-Zn may arise from the

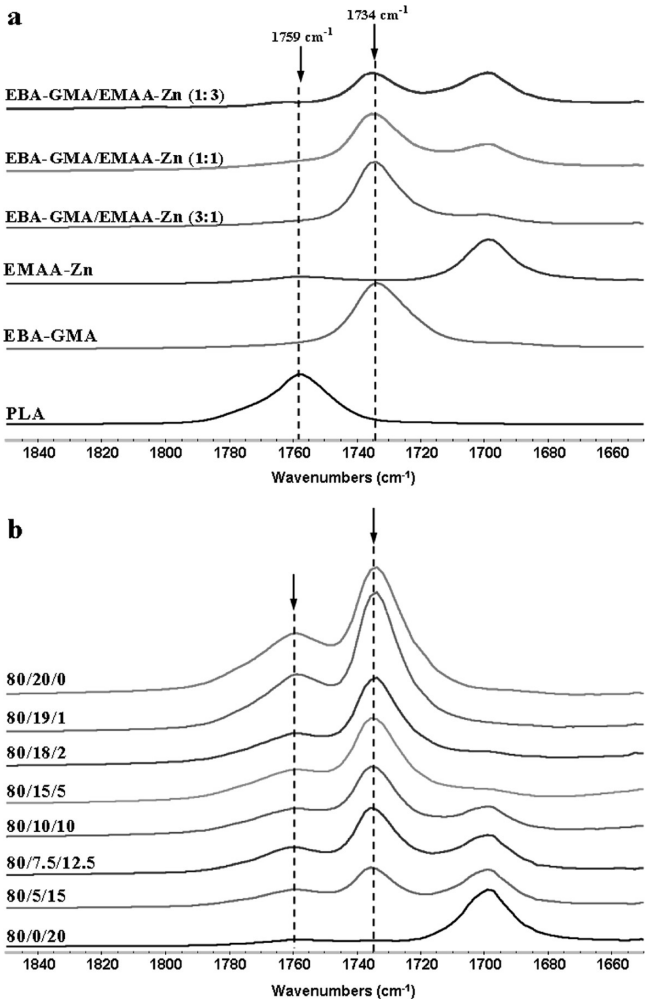

Figure 3. FT-IR absorption spectra in the range of 1650−1850 cm^{-1}: (a) individual polymers and EBA-GMA/EMAA-Zn binary blends; (b) residues from dioxane-extracted PLA/EBA-GMA/EMAA-Zn (80/20-x/x, w/w/w) blends having varying EBA-GMA/EMAA-Zn ratios.

formation of co-continuous phase morphology. The 90/10 binary blend exhibited the smallest slope, suggesting it had a slower cross-linking reaction rate than the other binary blends. The low reaction rate in this blend was probably attributed to the low EMAA-Zn content. Furthermore, as shown in Figure 2, the T_g of EBA-GMA in the blend where the EBA-GMA/EMAA-Zn ratio was 18/2 did not show a significant change compared with that of the neat EBA-GMA, suggesting that the cross-link density of the elastomer in this scenario was fairly low. Therefore, EBA-GMA in the 90/10 blend largely retained its thermoplastic characteristics, and the torque value did not drop as fast as in the case of the 75/25 blend after reaching the maximum value.

Figure 2 shows the damping factor as a function of temperature for various PLA/EBA-GMA/EMAA-Zn blends. Compared to the PLA/EBA-GMA binary blend, the T_g (i.e., α-transition) attributed to the EBA-GMA phase in the ternary blends exhibited little change with the addition of EMAA-Zn up to 2.0 wt %. This might suggest that the level of cross-linking of the EBA-GMA phase in these cases was still very low. With further addition of EMAA-Zn, however, the T_g of the EBA-GMA phase invariably shifted to a higher temperature and the damping peak also became broader, indicating the gradually increased restriction

Table 2. Crystallinity of the PLA Matrix and FT-IR Peak-Resolving Data of the Residues from Dioxane-Extracted PLA/EBA-GMA/EMAA-Zn (80/20-*x*/*x*, w/w) Blends

			PLA		EBA-GMA		
samples	EMAA-Zn (wt %)	X_c (%)	ν (cm^{-1})	A_{PLA}	ν (cm^{-1})	$A_{EBA\text{-}GMA}$	$A_{PLA}/A_{EBA\text{-}GMA}$
extruded PLA		0.2	1758.2				
extruded EBA-GMA					1733.9		
PLA/EBA-GMA/EMAA-Zn	0	6.5	1762.1	3.0	1733.1	5.3	0.56
	1.0	1.6	1761.1	5.1	1733.5	10.6	0.48
	2.0	0.6	1762.6	5.5	1733.7	14.9	0.37
	5.0	0.6	1763.1	2.6	1734.1	6.1	0.42
	10.0	1.0	1763.0	2.1	1734.5	4.3	0.48
	12.5	1.6	1762.3	5.0	1734.4	10.5	0.47
	15.0	3.4	1761.7	2.3	1735.0	3.7	0.62
	20.0	21.1					

of segment motion.[46] At 15 wt % EMAA-Zn, the T_g of the EBA-GMA phase was around ca. 20 °C, which was about 14 °C higher than that of the PLA/EBA-GMA binary blend. Cross-linking of the EBA-GMA phase as clearly evidenced by torque data should be responsible for such a continuous increase in T_g in these ternary blends. No change in T_g of the PLA matrix (~68 °C) with respect to neat PLA was noted, regardless of the EMAA-Zn loading levels. This result was in agreement with the DSC results (not shown).

FT-IR was utilized to analyze the reactive compatibilization at the PLA and EBA-GMA interfaces. Figure 3a shows the absorption spectra of individual polymers and binary EBA-GMA/EMAA-Zn blends in the range of 1650−1850 cm^{-1}. The absorption peaks at 1759 and 1734 cm^{-1} were attributed to the stretching vibration of carbonyl groups in the PLA and EBA-GMA, respectively. The EMAA-Zn ionomer exhibited a weak shoulder peak at 1757 cm^{-1} which was attributed to the free carboxylic acid groups and a strong absorption at 1700 cm^{-1} due to the carboxylic acid dimer.[47] As shown in Figure 3b, the spectrum of residues of the dioxane-extracted PLA/EMAA-Zn binary blend is closely identical to that of pure EMAA-Zn (Figure 3a), indicating the complete removal of the PLA component during dioxane extraction and further confirming the absence of interaction between these two immiscible components. Noticeably, the shoulder at 1759 cm^{-1} was still visible in the residues of all the blends after thorough extraction with dioxane for 10 days (Figure 3b), suggesting that PLA reacted with EBA-GMA during melt-blending. The resultant copolymers probably arose from the reaction of epoxy groups with end groups of PLA during melt-blending. A similar compatibilization reaction was also proposed in other PLA blend systems toughened by other epoxy-containing modifiers.[18,21,22,48] The extent of the compatibilization reaction can be approximately described by the amount of grafted PLA per unit of EBA-GMA used, as measured by the ratio of absorption peak area at 1759 cm^{-1} to that at 1734 cm^{-1}, i.e., $A_{PLA}/A_{EBA\text{-}GMA}$ (Table 2). Because the weak vibration peak of free carboxylic acid in EMAA-Zn was located at the almost same position as that of the ester carbonyl stretching vibration of PLA (ca. 1759 cm^{-1}), its relative contribution was evaluated in terms of the EBA-GMA/EMAA-Zn binary blends with different weight ratios (Figure 3a). It was found that even with high EMA-Zn content (i.e., EBA-GMA/EMAA-Zn = 1:3, w/w), free carboxylic acid groups of EMAA-Zn exhibited only a minor absorption area relative to that of the carbonyl groups of EBA-GMA at 1733 cm^{-1} (ca. 8%). Therefore, it was anticipated that the absorption at 1759 cm^{-1} primarily originated from ester carbonyl groups of PLA rather than free carboxylic acid groups of the ionomer, especially when EMAA-Zn content was below 15 wt % in the ternary blends. As shown in

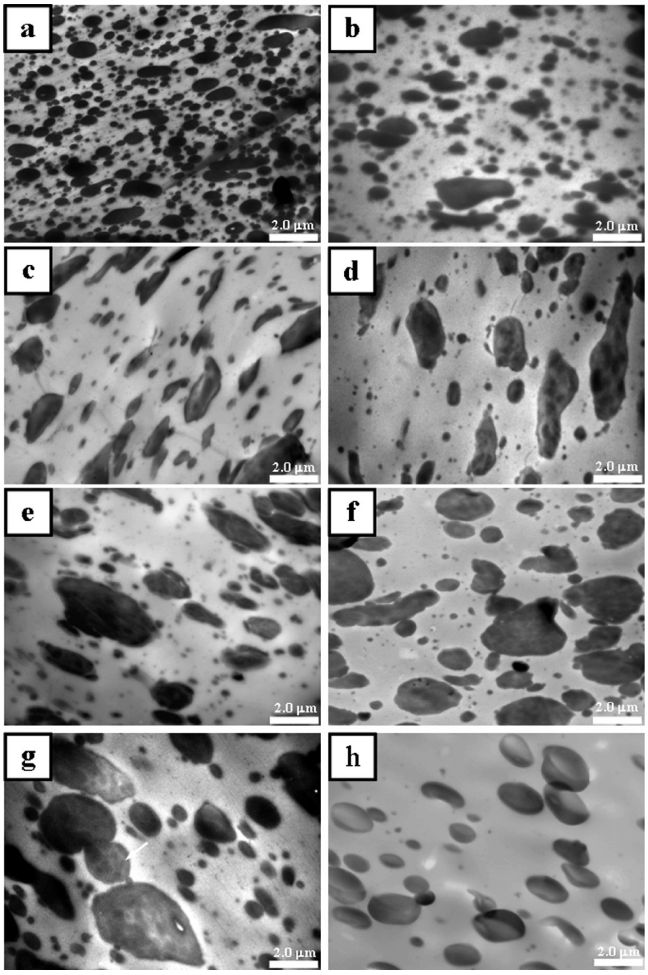

Figure 4. TEM images (low magnification) of PLA/EBA-GMA/EMAA-Zn (w/w/w) blends of different compositions: (a) 80/20/0; (b) 80/19/1; (c) 80/18/2; (d) 80/15/5; (e) 80/10/10; (f) 80/7.5/12.5; (g) 80/5/15; (h) 80/0/20.

Table 2, the $A_{PLA}/A_{EBA\text{-}GMA}$ values essentially remained in the comparable level for the ternary blends having varying EBA-GMA/EMAA-Zn; in other words, the increase in EMAA-Zn content did not remarkably diminish the extent of interfacial compatibilization between PLA and EBA-GMA. Also, it implied that the direct contact between PLA and EBA-GMA was likely to be well maintained during the interfacial compatibilization even though the ratio of EBA-GMA/EMAA-Zn was varied over a broad range.

3.2. Morphological Structure. Different magnifications of TEM micrographs of the ternary blends with varying EMAA-Zn content are shown in Figure 4 and Figure S1, respectively. With 1.0 wt % EMAA-Zn, the phase morphology of the ternary blend resembled that of the PLA/EBA-GMA binary blend except that the sizes of dispersed particles were larger in the former. When 2.0 wt % EMAA-Zn was added, the "salami"-like (i.e., domain-in-domain) dispersed phase structure began to appear, and the number of dispersed particles with irregular shapes increased. With further increasing EMAA-Zn content, the dark subinclusions became predominant within the "salami"-like domains. The area of the dark regions (Figure S1) in the dispersed "salami"-like domains was proportional to the volume fraction of EMAA-Zn. Further EDX analysis of this region also revealed the existence of a trace amount of the zinc element (Figure S2). At 10 wt % EMAA-Zn content or higher, it appeared that the EMAA-Zn phase gradually changed from occluded subinclusions into the outer continuous phase. The average particle size and its distribution of the dispersed phase were calculated and summarized in Table 3. It was found that the weight-average particle diameter, d_w, rapidly increased from 0.3 to 0.92 μm with the addition of EMAA-Zn up to 5.0 wt % and only changed slightly afterward. The particle size polydispersity, i.e., the ratios of d_w/d_n and d_v/d_n, was found to achieve the maximum values at the medium concentration of EMAA-Zn. Because both interfacial compatibilization and dynamic vulcanziation were involved, the factors determining final blend morphologies are far more complicated when compared to the blend systems that only involve compatibilizing reactions between the matrix and the dispersed phase. An in-depth investigation is still needed for better understanding this issue.

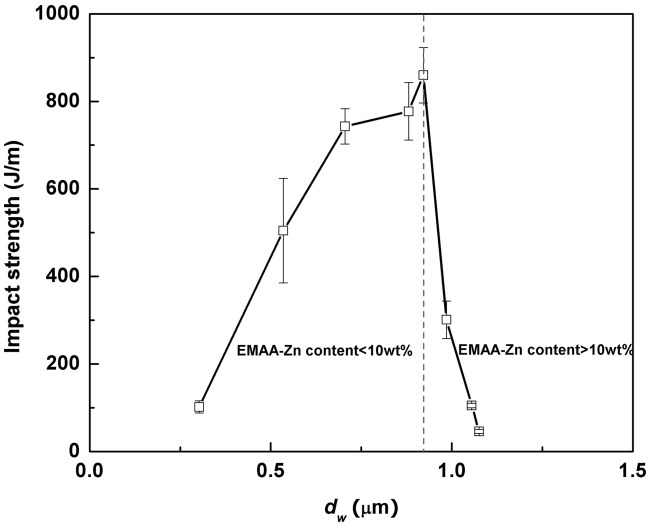

Figure 5. Izod impact strength of PLA/EBA-GMA/EMAA-Zn (80/20-x/x) blends with total content of both modifiers fixed at 20 wt % as a function of weight-average particle diameter (d_w).

In correspondence to the change of the substructure of dispersed particles, the wetting of the dispersed particles by the PLA matrix (Figure S3) began to deteriorate when the EMAA-Zn content exceeded 10 wt %. For the PLA/EBA-GMA/EMAA-Zn (80/5/15) ternary blend, interface wetting appeared very poor (Figure 6c and Figure S3f), which was somewhat similar to that in the PLA/EMAA-Zn binary blend (Figure S3g). Such change in interface wetting was consistent with the variation of the impact toughness (Table 3). As observed in the TEM results, the interfacial deterioration in the ternary blends containing more than 10 wt % EMAA-Zn was possibly attributed to the resulting EMAA-Zn shell layers with a poor affinity with the PLA matrix.

On the basis of the above results, Scheme 2 gives an illustration of the phase structure development for the PLA blend system. The equilibrium torque values (Figure 1) indicated that pure EBA-GMA had a comparable melt viscosity to that of pure EMAA-Zn; therefore, the large difference in the particle size between PLA/EBA-GMA and PLA/EMAA-Zn binary blends in Table 3 was probably attributed to a much lower interfacial tension of the former pair than that of the latter one. Since the dominant phase structure in multicomponent blends contained a minimization of interfacial free energy,[49−51] it was reasonably postulated that at the early stage of melt-blending the EMAA-Zn phase was preferentially encapsulated by EBA-GMA, which was dispersed in the PLA matrix regardless of the EBA-GMA/EMAA-Zn ratios. Such postulation was also evidenced by the above qualitative FT-IR analysis (Table 2), which suggested that the variation in EMAA-Zn content did not remarkably weaken the extent of interfacial compatibilization between PLA and EBA-GMA. On the other hand, good interfacial affinity was expected

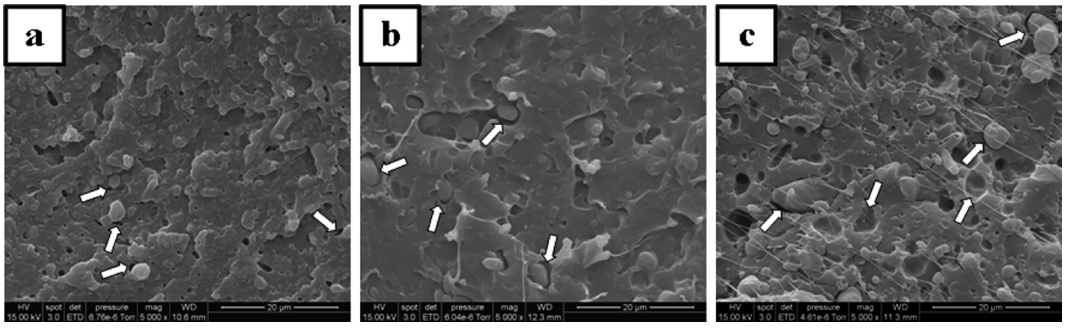

Figure 6. SEM micrographs of impact-fractured surface of PLA/EBA-GMA/EMAA-Zn blends adjacent to the notch: (a) 80/20/0; (b) 80/15/5; (c) 80/5/15.

Scheme 2. Proposed Morphology Evolution as a Function of EMAA-Zn Content in the PLA/EBA-GMA/EMAA-Zn (80/20-*x*/*x*, w/w/w) Blends

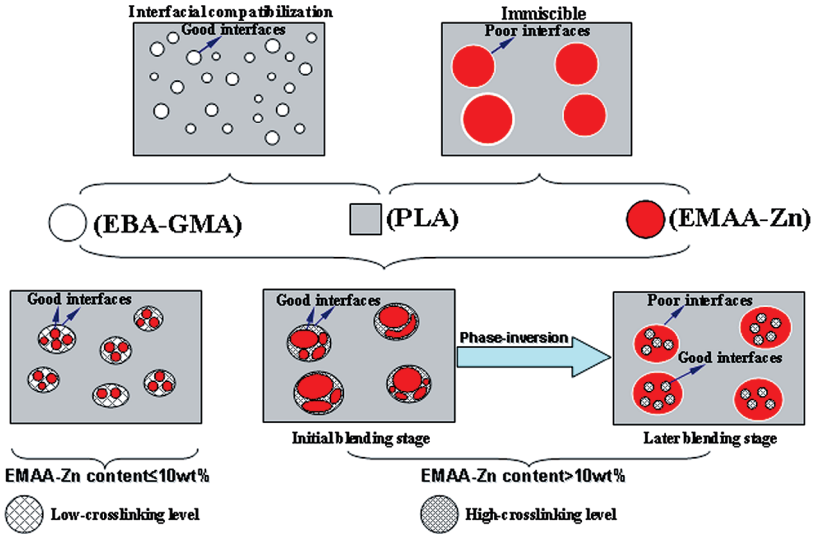

Table 3. Morphological Parameters and Impact Strength of Various PLA/EBA-GMA/EMAA-Zn (80/20-*x*/*x*, w/w) Blends

systems	EMAA-Zn (wt %)	impact strength (J/m)	d_w (μm)	d_w/d_n	d_v/d_n
neat PLA		24.6 ± 4.7			
x% EMAA-Zn + (20 − *x*)% EBA-GMA	0	101.9 ± 13.9	0.30	1.37	2.37
	1.0	504.9 ± 119.4	0.53	1.56	2.81
	2.0	742.9 ± 40.2	0.71	1.60	3.15
	5.0	859.8 ± 63.5	0.92	2.39	6.32
	10.0	777.2 ± 65.8	0.88	1.77	4.42
	12.5	301.0 ± 43.0	0.99	2.16	4.83
	15.0	105.1 ± 5.3	1.06	1.83	4.13
	20.0	45.8 ± 4.7	1.08	1.37	1.78

to exist between EBA-GMA and EMAA-Zn because both of them tended to react with each other during vulcanization, as revealed by the torque data.

When there was more EBA-GMA than EMAA-Zn in the ternary blends, the minor MAA-Zn phase remained trapped inside the EBA-GMA phase, and good interfacial adhesion prevailed at both the EBA-GMA/EMAA-Zn and PLA/EBA-GMA interfaces. Also, because of an enhanced resistance to breakup arising from cross-linking of the EBA-GMA phase, the size of dispersed "salami"-like particles was evidently enlarged in this case. When more EMAA-Zn was added with respect to EBA-GMA, however, the remarkably elevated cross-linking level (as evidenced by DMA data) led to a rapid increase in melt viscosity of the minor EBA-GMA phase. At the later stage of melt-blending, the phase inversion within the "salami"-like domains would take place, and the more viscous EBA-GMA phase enveloping the EMAA-Zn phase at the beginning stage was engulfed by the less viscous EMAA-Zn phase instead. As a result, the majority portion of the *in situ* formed PLA-*g*-EBA-GMA copolymers which were initially at the interfaces between the EBA-GMA and PLA matrix were also occluded inside the EMAA-Zn domains surrounding the EBA-GMA phase. Because of the immiscibility between the resultant EMAA-Zn shell and the PLA matrix, their interfacial wetting inevitably became poor in this situation.

3.3. Relationship between Impact Toughness and Dispersed Morphologies. Figure 5 shows the notched Izod impact strength as a function of dispersed particle size (d_w) for a series of PLA/EBA-GMA/EMAA-Zn (80/20-*x*/*x*) blends. An optimum particle size range (ca. 0.7−0.9 μm) for toughening was identified for this blend system. The brittle−ductile transition at the upper size limit appeared sharper, as compared to that at the lower one. Likewise, the optimum particle size has also been reported in other thermoplastic matrices containing a variety of rubbers, such as semicrystalline nylon-6 (PA6: 0.2−0.5 μm),[25−27] amorphous nylon (a-PA: 0.2−0.5 μm),[28] PMMA (0.2−0.3 μm),[29−31] PVC (0.2 μm),[32,33] poly(styrene-*co*-acrylonitrile) (SAN: 0.75 μm),[23] and polystyrene (PS: 1−2.5 μm).[23,34] Wu correlated rubber particle diameter with chain structure parameter of the matrix and claimed that the optimum particle size for toughening decreased as the matrix becomes less brittle.[23] Because PLA exhibited relatively higher intrinsic brittleness (characteristic chain ratio as a measure of chain flexibility, C_∞ = 9.5−11.8[52−54] depending on the L/D lactide ratio) than other matrices (e.g., C_∞ = 6.2 for PA6, C_∞ = 5.4 for a-PA, C_∞ = 7.6 for PVC, C_∞ = 8.2 for PMMA, C_∞ = 10.6 for SAN, and C_∞ = 10.8 for PS),[23,55] this optimum particle size for our toughened PLA

dx.doi.org/10.1021/ma1026934 |*Macromolecules* 2011, 44, 1513–1522

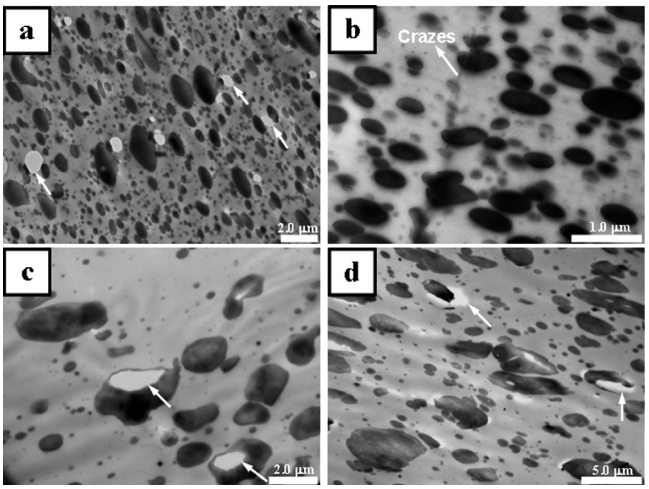

Figure 7. TEM micrographs of stress-whitening zone: (a) PLA/EBA-GMA (80/20) binary blend, low-magnification (×7500); (b) PLA/EBA-GMA (80/20) binary blend, high magnification (×30 000) at the localized area; (c) PLA/EBA-GMA/EMAA-Zn (80/15/5) ternary blend; (d) PLA/EBA-GMA/EMAA-Zn (80/5/15) ternary blend.

system seemed reasonable. Recently, by correlating tensile toughness with dispersed particle diameter in PLLA/conjugated soybean oil binary blends, Gramlich et al. also reported the similar range of optimum particle diameter (i.e., 0.5−0.9 μm) for toughening PLA.[15]

Since the crystallization of the PLA matrix could affect ultimate impact toughness of the blends,[19,21] the original crystallization state of the molded specimens was calculated from the thermograms of the first heating scan (Table 2). Except for the two binary PLA blends, the PLA crystallinity in all ternary blends was at a very low level (<4%). In the case of our ternary blend system, therefore, the difference in the PLA crystallinity hardly accounted for the remarkable dependence of impact toughness on the EBA-GMA/EMAA-Zn ratio.

3.4. Deformation Mechanism. Figure 6 shows SEM fractographs of the impact fractured surface of the blends in the vicinity of the notch. The surface of the PLA/EBA-GMA (80/20) binary blend exhibited some tiny voids but no clear plastic deformation in the matrix. Well-embedded particles in the matrix were also evidenced of good interfacial adhesion. Like the binary blend, good interfacial bonding also appeared in the ternary blend containing 5 wt % EMAA-Zn, but large cavities around the dispersed particles and a certain degree of matrix plastic deformation were noted in the ternary blend. In contrast, with the addition of 15 wt % EMAA-Zn, the debonding of coarse particles from the matrix prevailed and no perceptible plastic deformation of the matrix was observed. The fractographic observation of the above blends corresponded well to their impact strength.

TEM analysis of the subfracture surface was further employed to identify the micromechanical deformation process of the above samples (Figure 7). For the binary blend (Figure 7a), it was found that debonding mainly occurred around the relatively large particles, and no internal cavitation was observed. The formed microvoids often extended toward neighboring particles. Another important feature was the existence of minute fibrillated crazes passing through other neighboring particles under the higher magnification of a localized zone (Figure 7b). Therefore, when only EBA-GMA was used as a toughener, it appeared that debonding was insufficient to initiate the pervasive plastic deformation of the matrix required for high impact strength. On the contrary, extensive voiding inside the occluded elastomer particles was noticed in the PLA/EBA-GMA/EMAA-Zn (80/15/5) ternary blend (Figure 7c). And the internal cavitation seemed to preferably locate inside the gray region corresponding to the EBA-GMA phase. This might be attributed to the lower cavitation resistance of EBA-GMA with respect to EMAA-Zn due to a much lower modulus of the former than the latter.[29,37,38,56] However, the situation was different in the PLA/EBA-GMA/EMAA-Zn (80/5/15) ternary blend (Figure 7d), where the debonding at the interface between the dispersed domain and the PLA matrix prevailed. Therefore, internal cavitation of the dispersed particles followed by the matrix shear yielding was possibly a predominant toughening mechanism rather than interfacial debonding which resulted in the optimum impact strength in our PLA blend system.

It is generally accepted that microvoiding is the essential step which triggers matrix shear yielding, thereby resulting in considerable energy dissipation.[57−60] Microvoiding can occur either by internal cavitation or debonding.[56,61,62] A suitable level of interfacial strength was also needed to achieve optimal impact toughness in polymer blends.[63] Low interfacial adhesion easily resulted in premature interfacial failure and hence rapid and catastrophic crack propagation,[30,63] whereas very strong adhesion was unfavorable for debonding and also delayed the occurrence of matrix yielding.[64] Given sufficient rubber cavitation, the triaxial stress state ahead of the advancing crack can be changed into the plane stress state.[57] The plane stress state favored the occurrence of matrix shear yielding rather than the triaxial state which favored crazing.

For the PLA/EBA-GMA binary blend, internal cavitation of rubber particles was unfavorable due to the high cavitation resistance of its small particles,[29,33,35−38] so the occurrence of matrix shear yielding was delayed. On the other hand, the buildup of triaxial stress initiated numerous crazes and minute cracks otherwise occurred. Because many particles in this case were too small to effectively terminate the growing crazes or bridge the crack surfaces to prevent its propagation,[63] these microvoids easily coalesced into fatal cracks. Consequently, the impact specimens were unable to develop a substantial yield zone before the crack growth from the notch tip brought the test to an end, eventually giving the blends inferior impact toughness. When small amounts of EBA-GMA (e.g., 5.0 wt %) was replaced by EMAA-Zn, good interfacial adhesion still prevailed. Nevertheless, the cavitation resistance of dispersed particles was markedly lowered due to the enlarged dispersed particle size and still relatively low cross-linking level of the EBA-GMA phase. After cavitations, the triaxial stress constraint was relieved and then massive plastic deformation of the neighboring matrix occurred.[61] When EMAA-Zn was further increased up to 15 wt %, the particle size only slightly increased as compared to the former (0.92 μm vs 1.06 μm). Because of poor interfacial adhesion caused by the phase inversion, however, the premature crack propagation failed to be effectively stabilized at the early stage of the impact test. As a result, prior to the occurrence of constraint relief, the cracks quickly passed through the weak interfaces and inevitably resulted in unstable and brittle failure. Also, the enhanced cavitation resistance of EBA-GMA particles due to their higher level of cross-linking[29,65] as suggested by DMA data was possibly another cause for inferior fracture toughness in this case.

4. CONCLUSIONS

The EBA-GMA/EMAA-Zn ratio played a critical role in determining phase morphology and the ultimate impact performance of PLA/EBA-GMA/EMAA-Zn (80/20-*x*/*x*, w/w/w) ternary blends. An increase in EMAA-Zn content led to faster vulcanization and progressively higher cross-linked level of the EBA-GMA phase. FTIR analysis suggested that the variation in EBA-GMA/EMAA-Zn ratio did not remarkably change the compatibilization between PLA and EBA-GMA. Morphology analysis demonstrated that by increasing EMAA-Zn content, the EMAA-Zn phase gradually turned from occluded subinclusions into a continuous phase within the dispersed "salami"-like domains. It was reasonably proposed that when the EMAA-Zn content was above 10 wt %, phase inversion within the substructure of the dispersed phase domains was likely to take place, which would account for the pronounced deterioration in interfacial wetting of the dispersed particles by the PLA matrix in these cases. The correlation between particle size and impact toughness revealed that there existed an optimum particle size for PLA toughening in this ternary blend system. It appeared that the crystallization of PLA was not a contributing factor in achieving the supertoughness in the ternary blends. Preliminary analysis of micromechanical deformation suggested that the high impact toughness observed for some of the ternary blends was attributed to the low cavitation resistance of dispersed particles coupled with suitable interfacial adhesion.

■ ASSOCIATED CONTENT

Ⓢ Supporting Information. High-magnification TEM images (Figure S1), TEM-EDX spectra (Figure S2), and cryo-fractured SEM images of PLA/EBA-GMA/EMAA-Zn blends (Figure S2). This material is available free of charge via the Internet at http://pubs.acs.org.

■ AUTHOR INFORMATION

Corresponding Author

*Tel (509) 335-8723; Fax (509) 335-5077; e-mail jwzhang@wsu.edu.

■ ACKNOWLEDGMENT

The authors are grateful for the financial support from the National Research Initiative of the USDA Cooperative State Research, Education and Extension Service, grant no. 2007-35504-17818.

■ REFERENCES

(1) Jiang, L.; Wolcott, M. P.; Zhang, J. *Biomacromolecules* **2006**, *7*, 199–207.
(2) Zhang, N.; Wang, Q.; Ren, J.; Wang, L. *J. Mater. Sci.* **2009**, *44*, 250–256.
(3) Wang, L.; Ma, W.; Gross, R. A.; McCarthy, S. P. *Polym. Degrad. Stab.* **1998**, *59*, 161–168.
(4) Semba, T.; Kitagawa, K.; Ishiaku, U. S.; Hamada, H. *J. Appl. Polym. Sci.* **2006**, *101*, 1816–1825.
(5) Noda, I.; Satkowski, M. M.; Dowrey, A. E.; Marcott, C. *Macromol. Biosci.* **2004**, *4*, 269–275.
(6) Schreck, K. M.; Hillmyer, M. A. *J. Biotechnol.* **2007**, *132*, 287–295.
(7) Harada, M.; Ohya, T.; Iida, K.; Hayashi, H.; Hirano, K.; Fukuda, H. *J. Appl. Polym. Sci.* **2007**, *106*, 1813–1820.
(8) Wang, R.; Wang, S.; Zhang, Y.; Wan, C.; Ma, P. *Polym. Eng. Sci.* **2009**, *49*, 26–33.
(9) Zhang, J.-F.; Sun, X. *Polym. Int.* **2004**, *53*, 716–722.
(10) Bhardwaj, R.; Mohanty, A. K. *Biomacromolecules* **2007**, *8*, 2476–2484.
(11) Lin, Y.; Zhang, K.-Y.; Dong, Z.-M.; Dong, L.-S.; Li, Y.-S. *Macromolecules* **2007**, *40*, 6257–6267.
(12) Li, Y.; Shimizu, H. *Macromol. Biosci.* **2007**, *7*, 921–928.
(13) Zhang, W.; Chen, L.; Zhang, Y. *Polymer* **2009**, *50*, 1311–1315.
(14) Robertson, M. L.; Chang, K.; Gramlich, W. M.; Hillmyer, M. A. *Macromolecules* **2010**, *43*, 1807–1814.
(15) Gramlich, W. M.; Robertson, M. L.; Hillmyer, M. A. *Macromolecules* **2010**, *43*, 2313–2321.
(16) Ho, C.-H.; Wang, C.-H.; Lin, C.-I.; Lee, Y.-D. *Polymer* **2008**, *49*, 3902–3910.
(17) Ishida, S.; Nagasaki, R.; Chino, K.; Dong, T.; Inoue, Y. *J. Appl. Polym. Sci.* **2009**, *113*, 558–566.
(18) Li, Y.; Shimizu, H. *Eur. Polym. J.* **2009**, *45*, 738–746.
(19) Anderson, K. S.; Lim, S. H.; Hillmyer, M. A. *J. Appl. Polym. Sci.* **2003**, *89*, 3757–3768.
(20) Anderson, K. S.; Hillmyer, M. A. *Polymer* **2004**, *45*, 8809–8823.
(21) Oyama, H. T. *Polymer* **2009**, *50*, 747–751.
(22) Su, Z.; Li, Q.; Liu, Y.; Hu, G.-H.; Wu, C. *Eur. Polym. J.* **2009**, *45*, 2428–2433.
(23) Wu, S. *Polym. Eng. Sci.* **1990**, *30*, 753–761.
(24) Paul, D. R.; Bucknall, C. B. *Polymer Blends*, 2nd ed.; Wiley: New York, 2000; Vol. 2, Chapter 25.
(25) zOshinski, A. J.; Keskkula, H.; Paul, D. R. *Polymer* **1992**, *33*, 268–283.
(26) Oshinski, A. J.; Keskkula, H.; Paul, D. R. *J. Appl. Polym. Sci.* **1996**, *61*, 623–640.
(27) Oshinski, A. J.; Keskkula, H.; Paul, D. R. *Polymer* **1996**, *37*, 4909–4918.
(28) Huang, J. J.; Keskkula, H.; Paul, D. R. *Polymer* **2006**, *47*, 639–651.
(29) Dompas, D.; Groeninckx, G. *Polymer* **1994**, *35*, 4743–4749.
(30) Cho, K.; Yang, J. H.; Park, C. E. *Polymer* **1997**, *38*, 5161–5169.
(31) Cho, K.; Yang, J. H.; Park, C. E. *Polymer* **1998**, *39*, 3073–3081.
(32) Takaki, A.; Yasui, H.; Narisawa, I. *Polym. Eng. Sci.* **1997**, *37*, 105–119.
(33) Dompas, D.; Groeninckx, G.; Isogawa, M.; Hasegawa, T.; Kadokura, M. *Polymer* **1994**, *35*, 4760–4765.
(34) Bucknall, C. B. In *Polymer Blends*; Paul, D. R., Newman, S., Eds.; Academic: New York, 1978; Vol. 2, pp 99−102.
(35) Bucknall, C. B.; Paul, D. R. *Polymer* **2009**, *50*, 5539–5548.
(36) Dompas, D.; Groeninckx, G.; Isogawa, M.; Hasegawa, T.; Kadokura, M. *Polymer* **1994**, *35*, 4750–4759.
(37) Lazzeri, A.; Bucknall, C. B. *J. Mater. Sci.* **1993**, *28*, 6799–6808.
(38) Dijkstra, K.; Van der Wal, A.; Gaymans, R. J. *J. Mater. Sci.* **1994**, *29*, 3489–3496.
(39) Liu, J.; Sue, H.-J.; Thompson, Z. J.; Bates, F. S.; Dettloff, M.; Jacob, G.; Verghese, N.; Pham, H. *Macromolecules* **2008**, *41*, 7616–7624.
(40) Liu, H.; Chen, F.; Liu, B.; Estep, G.; Zhang, J. *Macromolecules* **2010**, *43*, 6058–6066.
(41) Kaci, M.; Cimmino, S.; Silvestre, C.; Duraccio, D.; Benhamida, A.; Zaidi, L. *Macromol. Mater. Eng.* **2006**, *291*, 869–876.
(42) Shah, R. K.; Paul, D. R. *Macromolecules* **2006**, *39*, 3327–3336.
(43) Oshinski, A. J.; Keskkula, H.; Paul, D. R. *Polymer* **1996**, *37*, 4891–4907.
(44) van der Wal, A.; Verheul, A. J. J.; Gaymans, R. J. *Polymer* **1999**, *40*, 6057–6065.
(45) Garlotta, D. *J. Polym. Environ.* **2001**, *9*, 63–84.
(46) Nielson, L. E.; Landel, R. F. *Mechanical Properties of Polymers and Composites*, 2nd ed.; Marcel Dekker: New York, 1994.
(47) Coleman, M. M.; Lee, J. Y.; Painter, P. C. *Macromolecules* **1990**, *23*, 2339–2345.
(48) Su, Z. Z.; Li, Q. Y.; Liu, Y. J.; Xu, H. Y.; Guo, W. H.; Wu, C. F. *J. Macromol. Sci., Part B: Phys.* **2009**, *48*, 823–833.

(49) Hobbs, S. Y.; Dekkers, M. E. J.; Watkins, V. H. *Polymer* **1988**, *29*, 1598–1602.
(50) Guo, H. F.; Packirisamy, S.; Gvozdic, N. V.; Meier, D. J. *Polymer* **1997**, *38*, 785–794.
(51) Guo, H. F.; Gvozdic, N. V.; Meier, D. J. *Polymer* **1997**, *38*, 4915–4923.
(52) Grijpma, D. W.; Pennings, J. P.; Pennings, A. J. *Colloid Polym. Sci.* **1994**, *272*, 1068–1081.
(53) Joziasse, C. A. P.; Veenstra, H.; Grijpma, D. W.; Pennings, A. J. *Macromol. Chem. Phys.* **1996**, *197*, 2219–2229.
(54) Cooper-white, J. J.; Mackay, M. E. *J. Polym. Sci., Part B: Polym. Phys.* **1999**, *37*, 1803–1814.
(55) Wu, S. *Polym. Int.* **1992**, *29*, 229–247.
(56) Borggreve, R. J. M.; Gaymans, R. J.; Eichenwald, H. M. *Polymer* **1989**, *30*, 78–83.
(57) Yee, A. F.; Li, D. M.; Li, X. W. *J. Mater. Sci.* **1993**, *28*, 6392–6398.
(58) Bucknall, C. B.; Soares, V. L. P.; Yang, H. H.; Zhang, X. C. *Macromol. Symp.* **1996**, *101*, 265–271.
(59) Kim, G. M.; Michler, G. H. *Polymer* **1998**, *39*, 5689–5697.
(60) Kim, G. M.; Michler, G. H. *Polymer* **1998**, *39*, 5699–5703.
(61) Sue, H.-J.; Huang, J.; Yee, A. F. *Polymer* **1992**, *33*, 4868–4871.
(62) Dompas, D.; Groeninckx, G.; Isogawa, M.; Hasegawa, T.; Kadokura, M. *Polymer* **1995**, *36*, 437–441.
(63) Wu, J. S.; Mai, Y.-W.; Yee, A. F. *J. Mater. Sci.* **1994**, *29*, 4510–4522.
(64) Liu, Z.; Zhu, X.; Wu, L.; Li, Y.; Qi, Z.; Choy, C.; Wang, F. *Polymer* **2001**, *42*, 737–746.
(65) Steenbrink, A. C.; Litvinov, V. M.; Gaymans, R. J. *Polymer* **1998**, *39*, 4817–4825.